

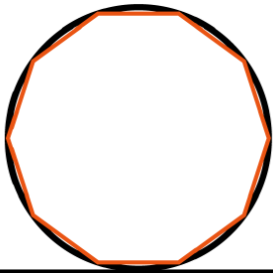
CLEO:2019 (STh4J.6)

May 9, 2019

Ultrahigh-Q Crystalline Microresonator Fabricated with Computer-controlled Machining without Polishing

Shun Fujii¹, Mika Fuchida¹, Hikaru Amano², Ryo Suzuki¹,
Yasuhiro Kakinuma², and Takasumi Tanabe¹

1. Department of Electronics and Electrical Engineering,
Faculty of Science and Technology, Keio University
2. Department of System Design Engineering,
Faculty of Science and Technology, Keio University

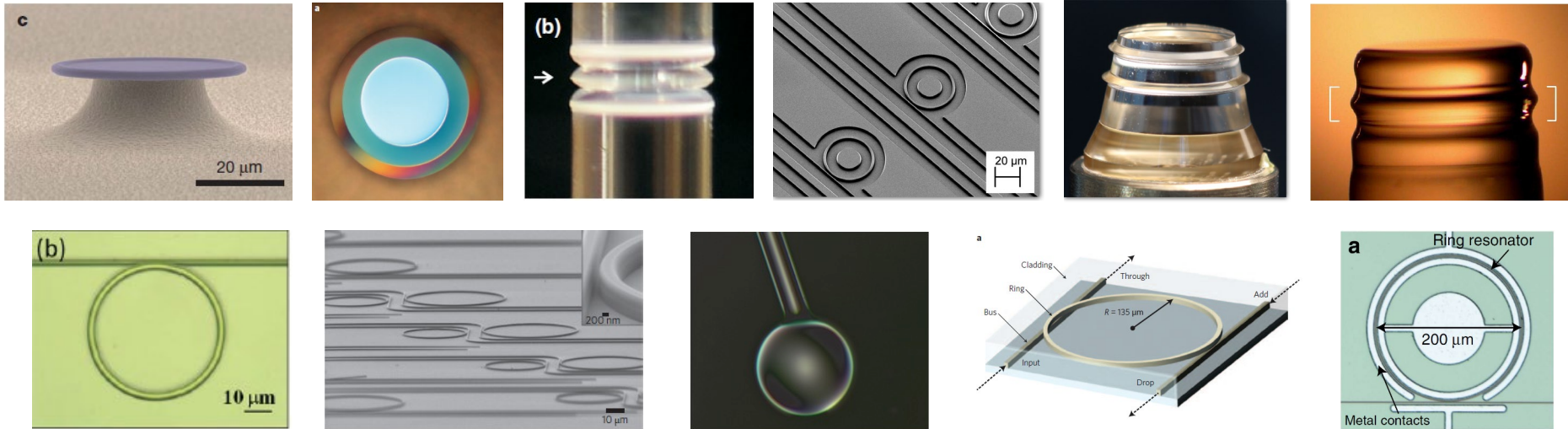


Whispering gallery mode (WGM) optical microresonator

Confines light for long photon lifetime (high Q) and has small volume

Enhances light-matter interaction in dielectric material

Dielectric microresonator platforms (Caltech, NIST, EPFL, OEwaves, Columbia, Harvard, Yale, INRS-EMT)



$$(\text{Intracavity power}) = \frac{4\eta d_1 Q}{\omega_0} \times (\text{Input power})$$

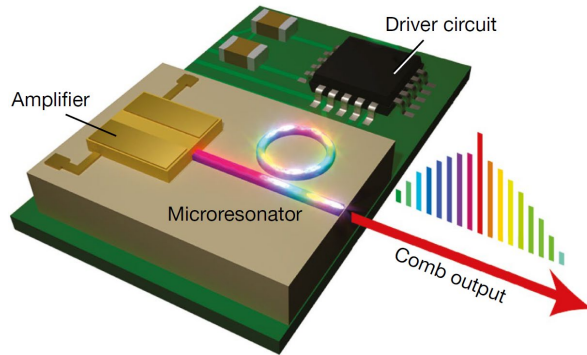
ω_0 : laser frequency, d_1 : cavity FSR,
 Q : quality factor, η : coupling parameter

e.g. $\omega_0/2\pi = 193$ THz, $d_1 = 100$ GHz,
 $Q = 1 \times 10^8$, $\eta = 0.5$ (critical coupling)

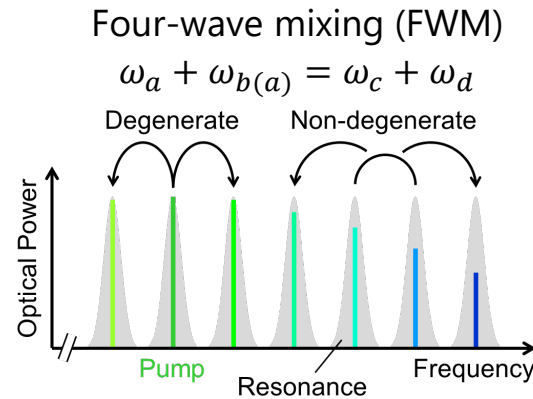
10 mW input \Rightarrow 165 W intracavity



Target application: Microresonator frequency comb (Kerr comb)



Nature 562, 401–405 (2018)



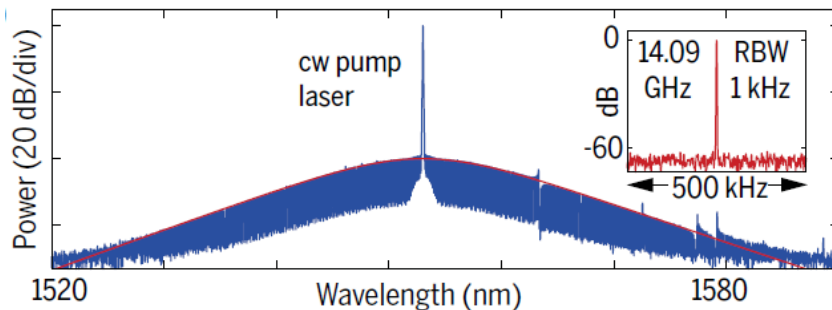
Threshold power for FWM

$$P_{\text{th}} = \frac{\kappa^2 n_0^2 V_{\text{eff}}}{8\eta\omega_0 c n_2} \propto \frac{V}{n_2 Q^2}$$

- Compact size
- Low energy consumption
- Broad bandwidth
- Large mode spacing ~ 1000 GHz

Optical spectrum of soliton

Science 361, 8083 (2018)

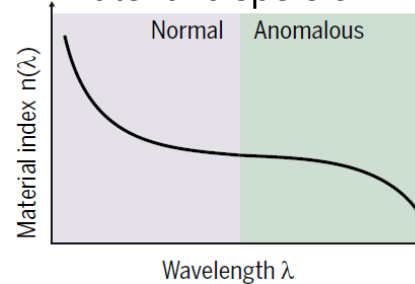


- Mode-locked state in Kerr comb (Kerr soliton)

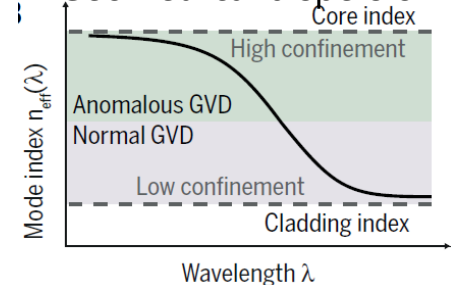
$$\Psi(\mu) = \sqrt{d_2/2} \operatorname{sech} \left(\frac{\pi\mu}{2} \sqrt{\frac{d_2}{\zeta_0}} \right) \quad \begin{aligned} d_2 &= D_2/\kappa \\ \zeta_0 &= \pi^2 f^2/8 \end{aligned}$$

Microresonator dispersion

Material dispersion



Geometrical dispersion



- Anomalous dispersion condition required

$$\beta_2 < 0 \quad (D_2 > 0) \quad \beta_2 = \frac{d^2\beta}{d\omega^2} = -\frac{nD_2}{cD_1^2}$$



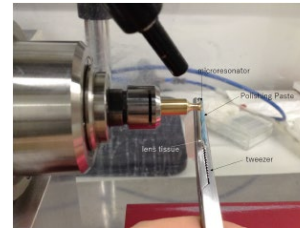
Mainstream microresonator fabrication methods



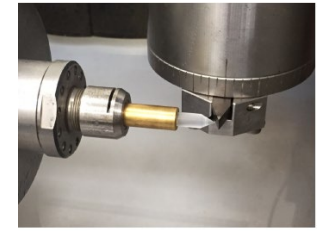
CO₂ laser reflow



Chemical etching



Polishing



Machining

Silica (SiO₂)
Toroid / Sphere / Rod

Q ~ 10⁸

Only amorphous
Geometric control ✗

Silica (SiO₂) disk
Silicon nitride (SiN)
Diamond Silicon (Si)

Q ~ 10⁷

Various materials
Geometric control ○

Fluoride crystal
MgF₂ CaF₂ BaF₂
LiNbO₃(PPLN)

Q ~ 10¹⁰

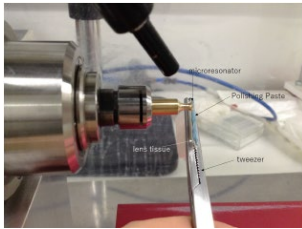
Ultra-high Q
Geometric control ✗

Q ~ 10⁶

Low Q
Geometric control ○



Combination of two methods



Polishing



Machining

Fluoride crystal

MgF_2 CaF_2 BaF_2

LiNbO_3 (PPLN)

$Q \sim 10^{10}$

$Q \sim 10^6$

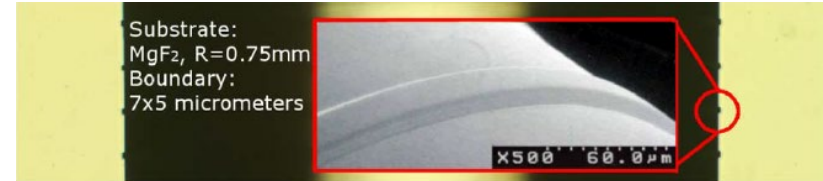
Ultra-high Q

Low Q

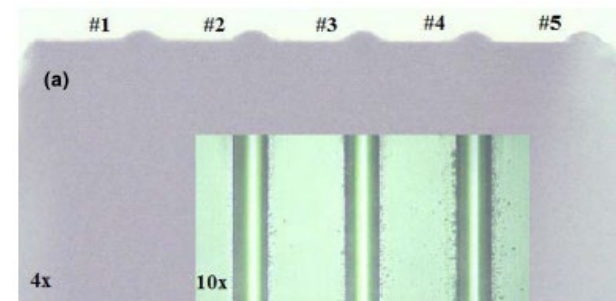
Form accuracy ✘

Form accuracy ○

Crystalline resonators formed by hand polishing after diamond turning process (Q exceeding 10^8)



Optica 2, 221 (2015)



Optics Letters 42, 514 (2017)

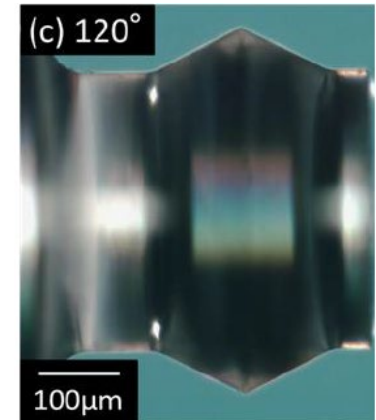
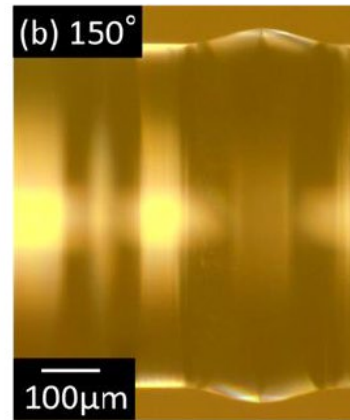
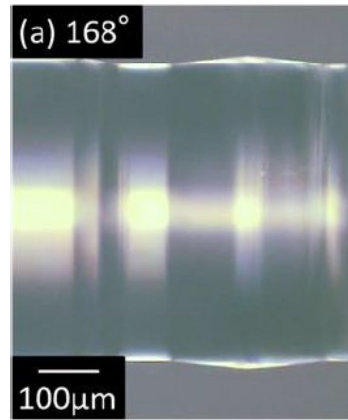
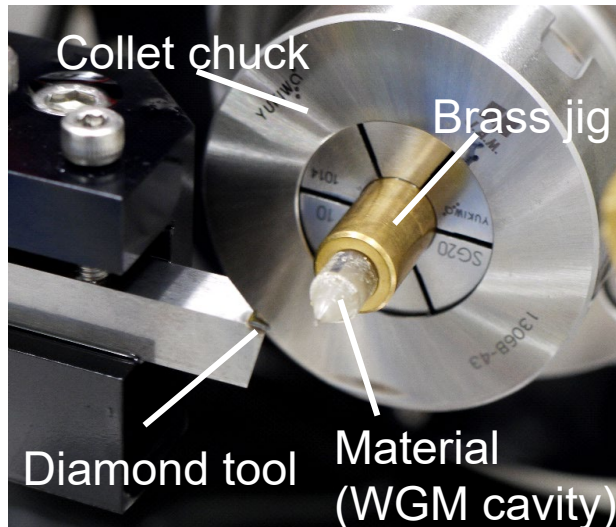
- Ultra-high Q ($Q > 10^9$) achieved by polishing after computer-controlled machining process
- Additional hand polishing degrades predesigned geometry (disadvantage for dispersion tailoring)
- Never again producing the standard microresonators



Motivation

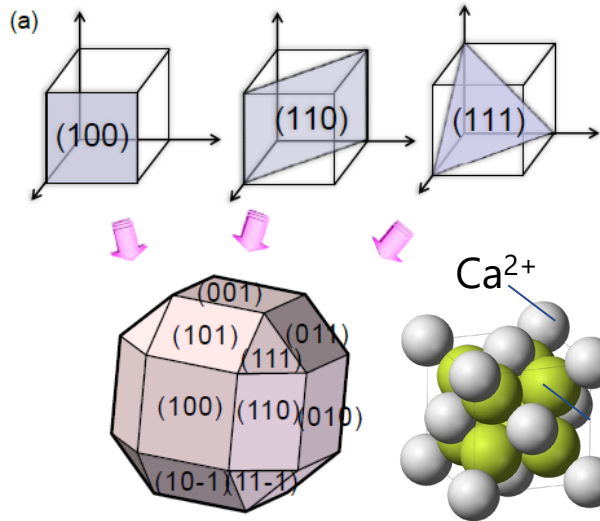
- Fabricate ultra-high Q crystalline microresonators ($Q > 10^8$) by computer-controlled machining **without polishing**
- Explore the potential of dispersion engineering for crystalline microresonators towards soliton formation at broadband wavelengths

Fully computer-controlled ultra-precision machining for dispersion engineering



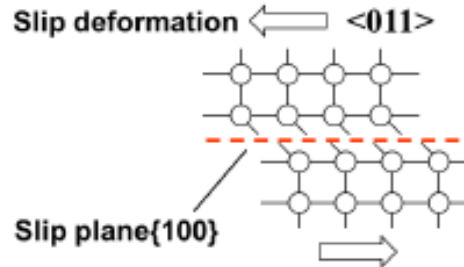


Crystallographic image of CaF_2 material



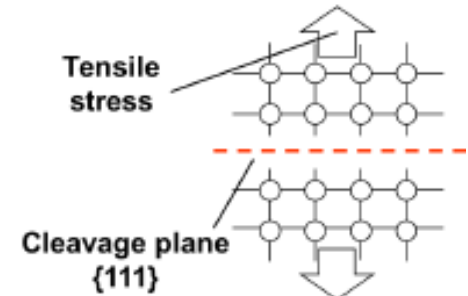
- Plane of single crystal is defined as mirror index
- CaF_2 consists of only 3 planes (100), (110), (111)
- Cutting mode transition observed with cutting depth

Slip formation (100)[110]



More ductile

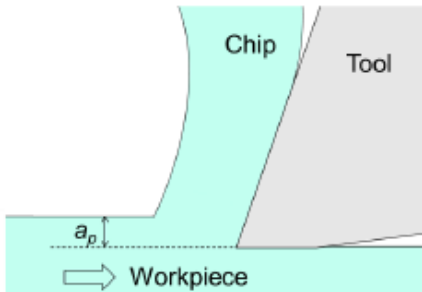
Cleavage formation (111)



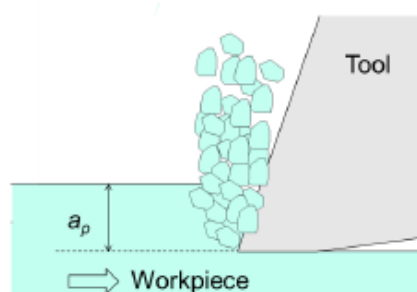
Very brittle

Cutting mode transition is observed depending on crystal anisotropy

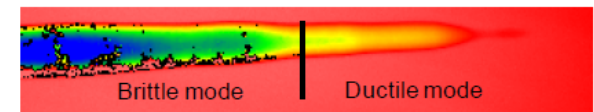
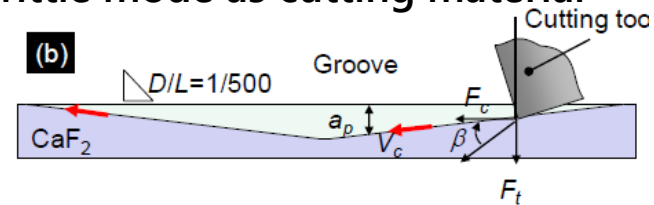
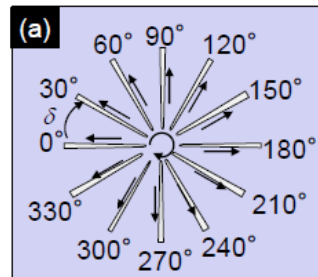
Ductile-mode cutting



Brittle-mode cutting



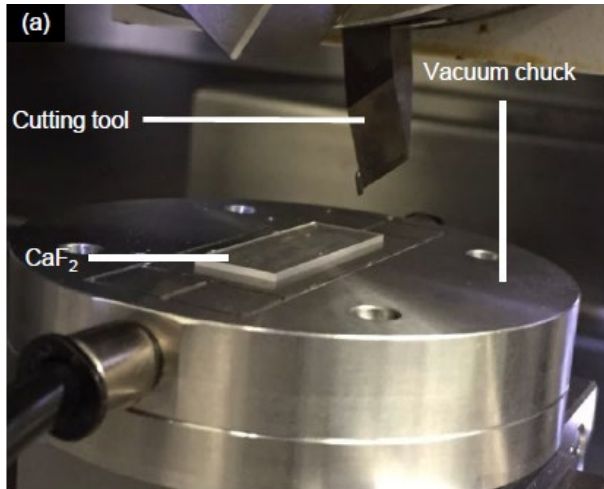
Transition to brittle mode as cutting material



Cutting depth < Critical depth Cutting depth > Critical depth



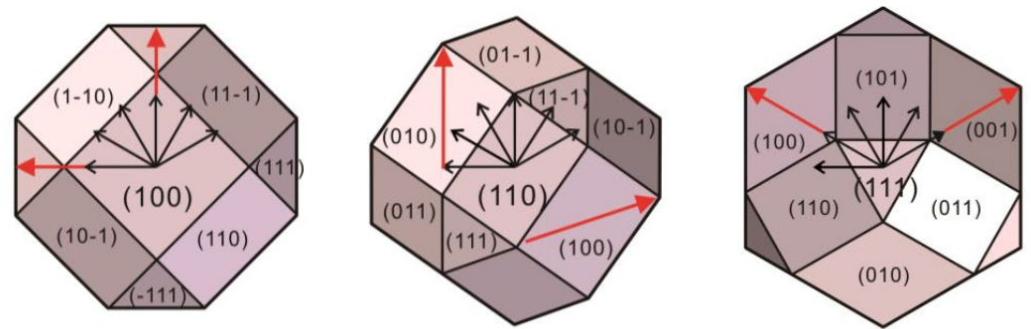
Experimental setup



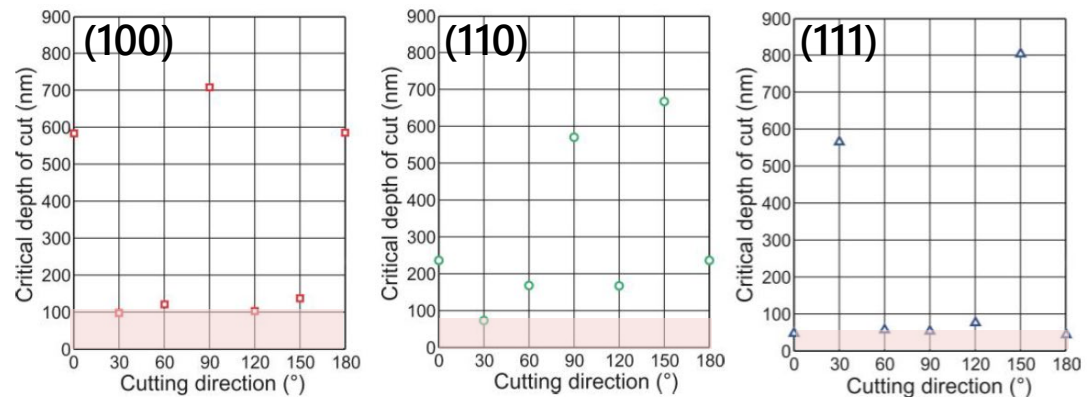
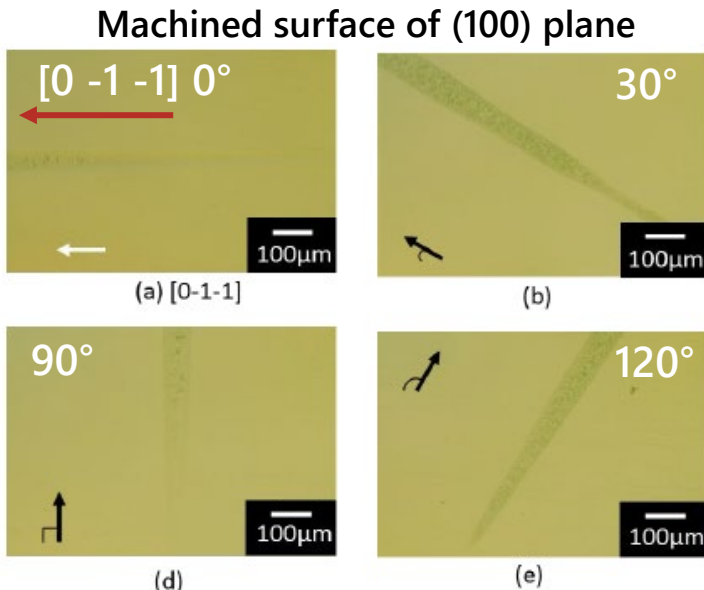
“Objective” of orthogonal cutting experiment

- Resonators must be fabricated with ductile-mode cutting
- Identify critical cutting depth for all crystal planes and cutting directions with orthogonal cutting experiment

Critical cutting depth vs direction for different planes



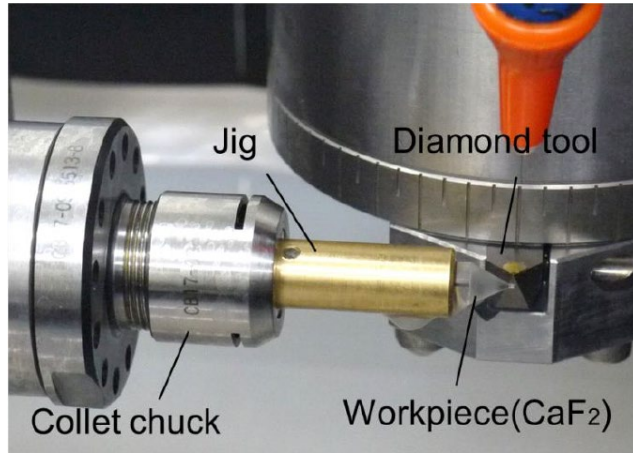
← Slip system ← Cutting direction



Critical cutting depth is over 50 nm for all planes

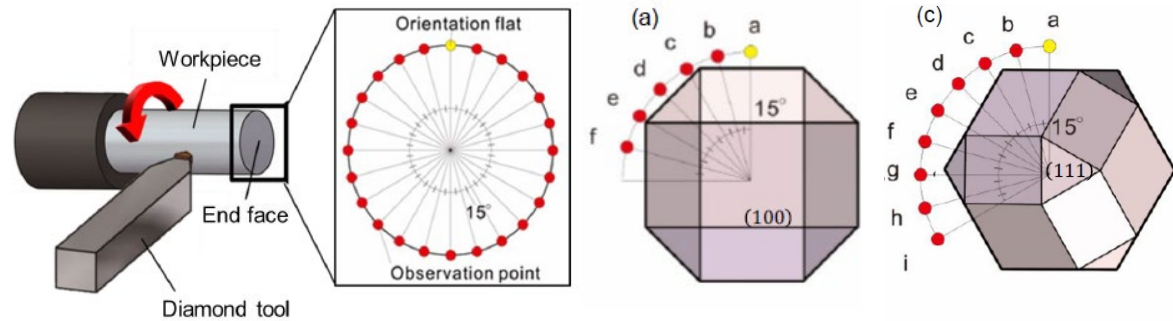


Experimental setup

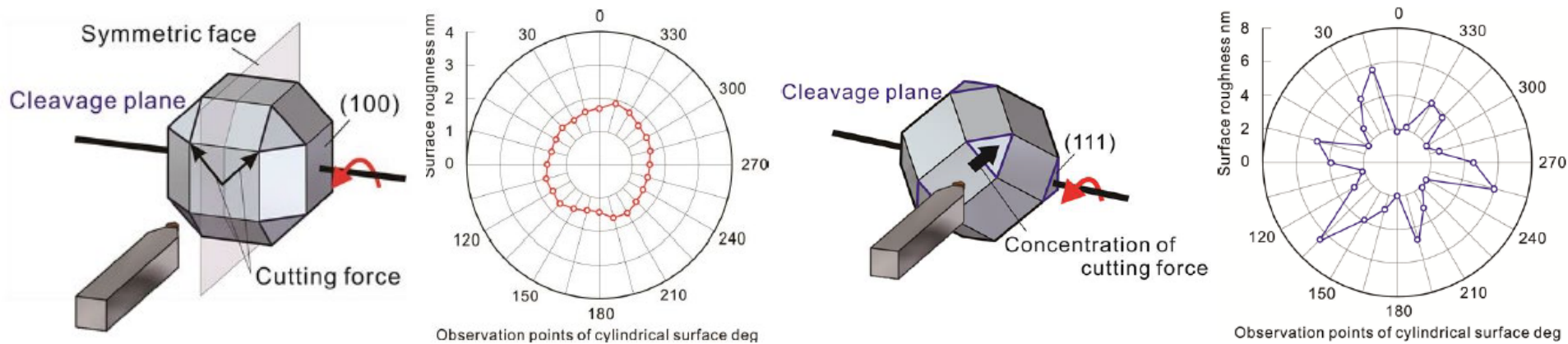


“Objective” of cylindrical turning experiment

- Cutting plane and direction are continuously and simultaneously changed when resonator is turned
- Investigate surface roughness of entire cylindrical surface



Cylindrical surface roughness for observation points with different end-faces

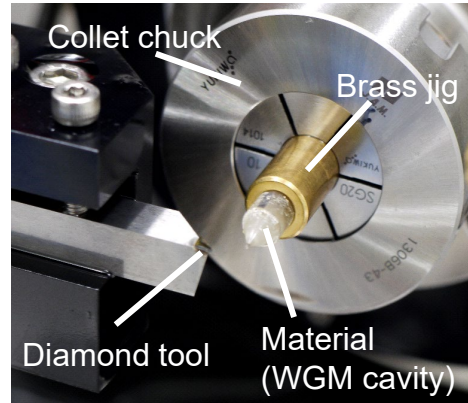


Observed smooth surface with end-face (100)

Observed surface clack with the end-face (111)



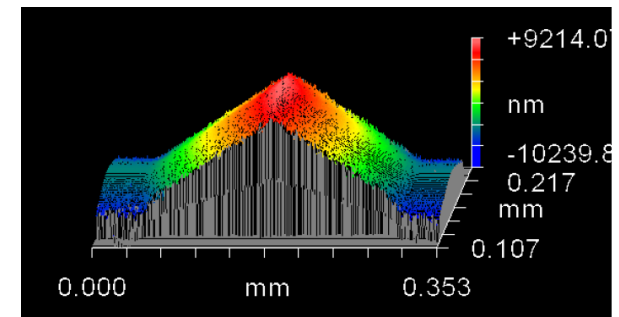
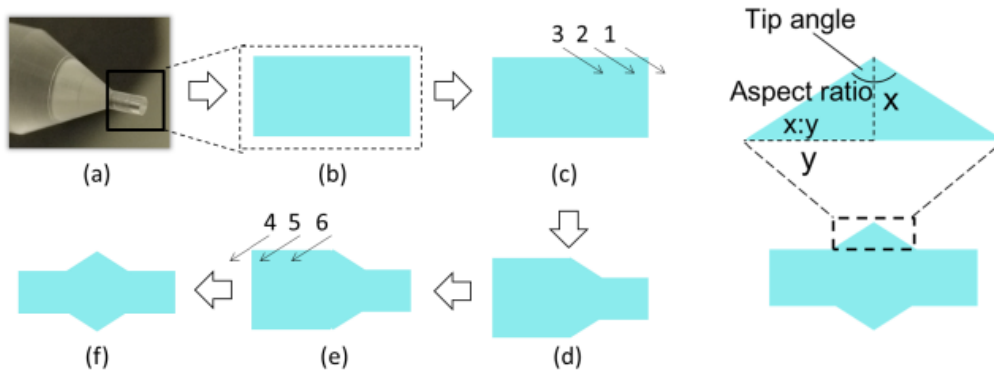
Experimental setup and machine used



Manufacturing parameters

- Rotation speed [min^{-1}]
- Cutting speed [m/min]
- Feed per revolution [$\mu\text{m}/\text{rev}$]
- Depth of cut [nm]
- End-face orientation
- Lubricant
- Nose radius (cutting tool)
- Rake angle (cutting tool)

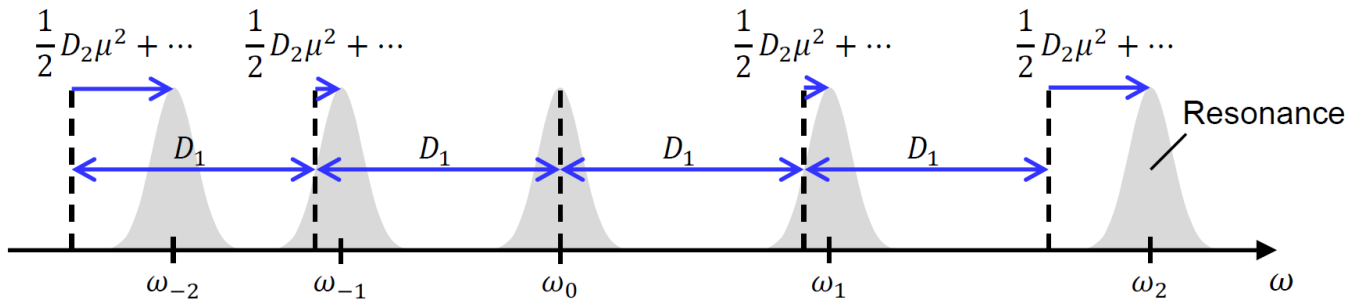
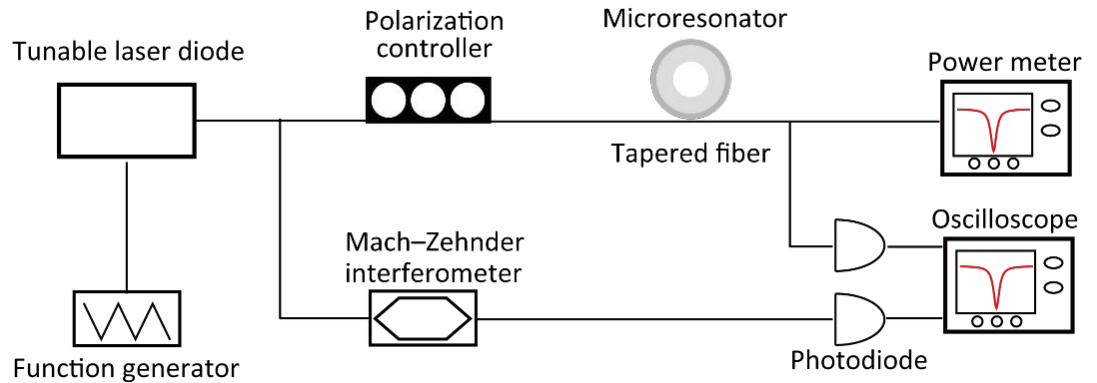
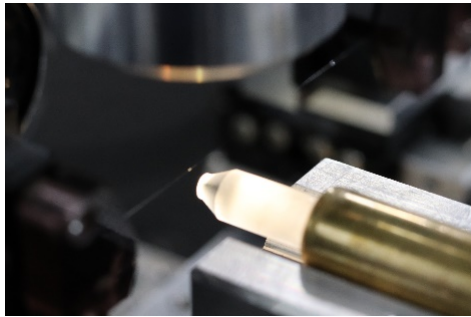
Fabrication flow of ultra-precision turning for *triangular* cross-section microresonator



- The tip angle and the aspect ratio are pre-designed and formed by computer-controlled turning, which is attractive with respect to dispersion engineering



Experimental setup for Q-factor and dispersion measurement



Group-velocity dispersion

$D_2 > 0$: anomalous
 $D_2 < 0$: normal

Resonance frequency:
$$\omega_m = \frac{2\pi mc}{Ln(\omega)}$$

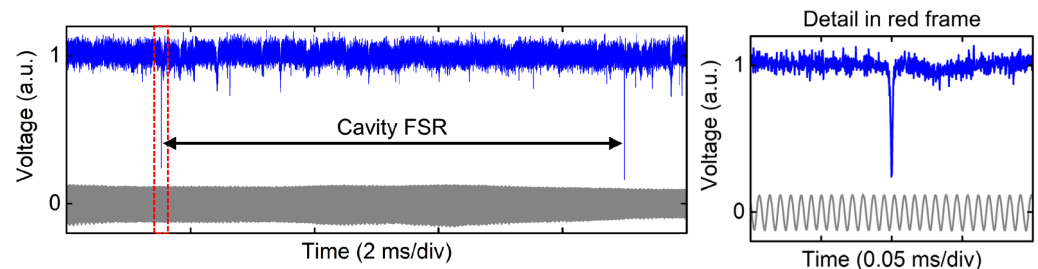
Resonance frequencies are Taylor-expanded:

$$\omega_\mu = \omega_0 + D_1\mu + \frac{1}{2}D_2\mu^2 + \frac{1}{6}D_3\mu^3 + \dots$$

m : mode number

μ : mode number offset (from pump $\mu = 0$)

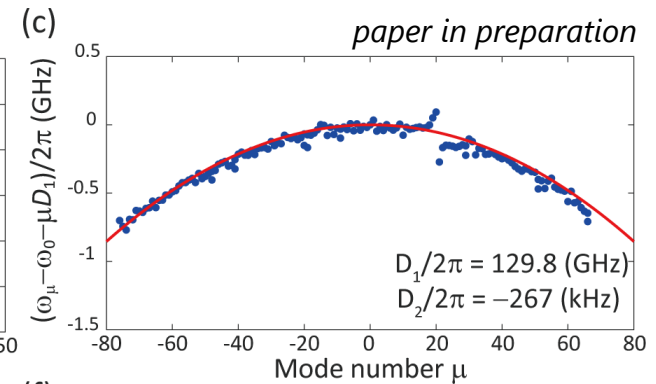
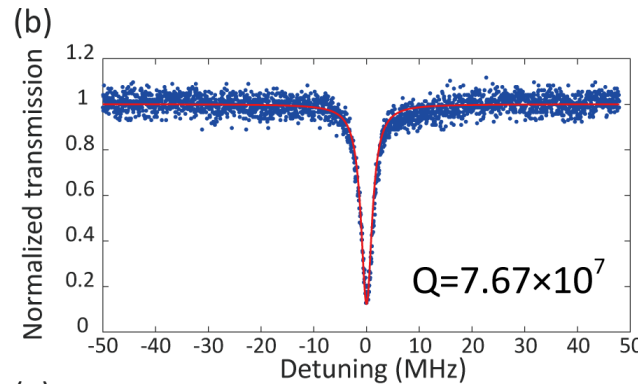
Mach-Zehnder interferometer calibrates frequency axis



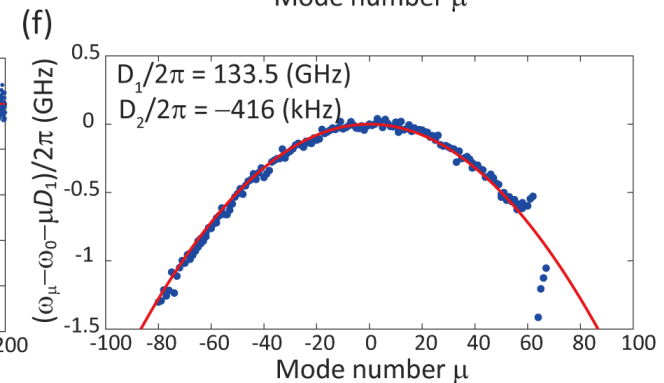
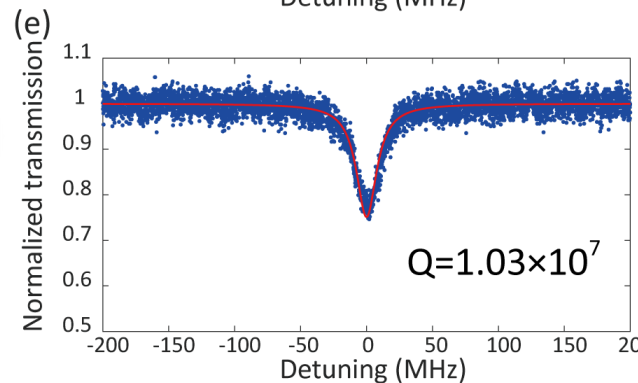


CaF₂ crystalline microresonator fabricated "*without polishing*"

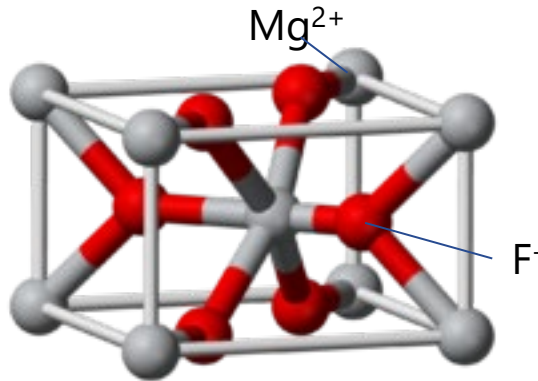
Spherical WGM
Diameter 512 μm
Curvature 36 μm



Triangular WGM
Diameter 502 μm
Apex angle 120°



- Measurements were performed after removing chips by cleaning with lens tissue
- Experimental measured dispersions agree well with simulation results
- Spherical cross-sectional shape shows higher Q than triangular shape



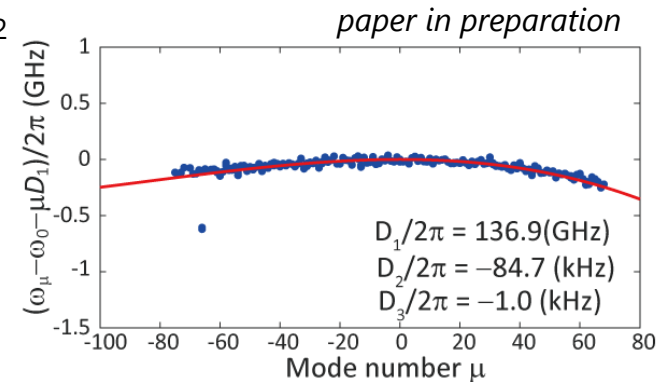
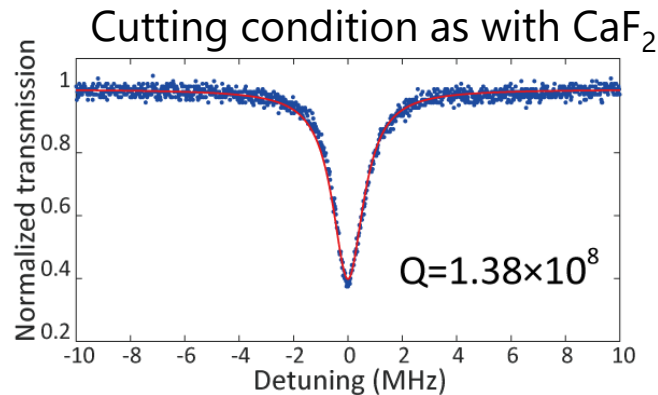
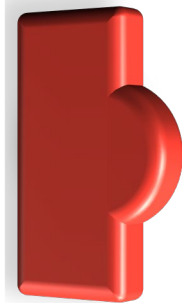
Magnesium fluoride has a “rutile” structure

- Crystallographic image is more complex than that of CaF_2
- Cutting condition will also be complex...

Knoop hardness (hardness of a materials)

- MgF_2 : 415 (kg/mm^2)
- CaF_2 : 158.3 (kg/mm^2)

Spherical WGM
Diameter 508 μm
Curvature 36 μm






- Highest Q-factor exceeding 10^8 was observed in MgF_2 spherical WGM resonator
- Effect of crystal anisotropy and best end-face should be investigated
- MgF_2 is more suitable for Kerr comb generation as regards thermal stability



- Investigated machining of single crystal material
- Identified critical depth and for each end-face orientation to achieve ultra-precision machining of CaF₂ WGM microresonators
- Observed highest Q exceeding 10⁸ without polishing process

Summary of crystalline microresonators fabricated without polishing

| | | | | |
|---|---------------------------------|----------------------------|-----------------|--------------------------------|
|  | CaF ₂ Spherical WGM | Q = 7.67 × 10 ⁷ | FSR = 129.8 GHz | D ₂ /2π = -267 kHz |
| | | Q = 6.07 × 10 ⁷ | FSR = 22.08 GHz | D ₂ /2π = -2.3 kHz |
|  | CaF ₂ Triangular WGM | Q = 1.03 × 10 ⁷ | FSR = 133.5 GHz | D ₂ /2π = -416 kHz |
|  | MgF ₂ Spherical WGM | Q = 1.38 × 10 ⁸ | FSR = 136.9 GHz | D ₂ /2π = -84.7 kHz |
| | | Q = 2.1 × 10 ⁷ | FSR = 21.61 GHz | D ₂ /2π = 4.86 kHz |

Thank you

Acknowledgment

This work is supported by Japan Society for the Promotion of Science (JSPS) KAKENHI under Grant Number JP19H00873, JP18J21797 and Grant-in-Aid for JSPS Fellow; Amada Foundation; The Ministry of Education, Culture, Sports, Science and Technology (MEXT) Q-LEAP

We thank Dr. Y. Mizumoto, H. Kangawa, and Ms. Y. Hayama for their contribution of this work